Korean J. Chem. Eng., 34(3), 681-691 (2017)
DOI: 10.1007/s11814-016-0327-8

pISSN: 0256-1115
eISSN: 1975-7220

Two-stage cracking catalyst of amorphous silica-alumina on Y zeolite for enhanced product selectivity and suppressed coking

Mahdi Davoodpour*, Reza Tafreshi*, Abbas Ali Khodadadi*,,†, and Yadolla Mortazavi*,****

*Catalysis and Nanostructured Materials Research Laboratory, School of Chemical Engineering, University of Tehran, P. O. Box 11155/4563, Tehran, Iran
**Oil and Gas Center of Excellence, P. O. Box 11155/4563, University of Tehran, Tehran, Iran
(*Received 2 August 2016 • accepted 20 November 2016*)

Abstract−A novel bilayer catalyst composed of amorphous silica-alumina (ASA) layer coated on Y zeolite layer is proposed as a fluid catalytic cracking (FCC) catalyst to cause two-stage reactions of pre-cracking and deep-cracking. The bilayer catalyst (Y/ASA) is compared with the usual mixed one (ASA+Y), in catalytic cracking of a feed composed of 1,3,5-triisopropylbenzene and naphthalene. The two catalyst representations were prepared by applying layers of Y zeolite and ASA or both on inert monolith supports. Catalytic cracking experiments were carried out at 300, 350 and 400 °C. Compared to Y+ASA, Y/ASA yielded about 33% and 46% more benzene and toluene, respectively, and 18% less coke in the catalytic cracking at 350 °C. The coke of Y/ASA was less refractory than that of Y+ASA as burnt at lower temperatures, while emitting less carbon monoxide in regeneration. Y/ASA configuration shows promising features as FCC catalysts for increased bottoms cracking and suppressed coking.

Keywords: FCC, Preliminary Cracking, Coke, Acid Sites, Silica-alumina

INTRODUCTION

Fluid catalytic cracking (FCC), as a well proven refinery process, has recently focused on utilization of higher content of residual cuts. The fluctuations in oil price, on one hand and the decrease in the quality of conventional crude oils on the other hand, has motivated the refiners to consider more residue processing in FCC units [1,2], a process which is particularly distinguished as resid FCC/RFCC. The residua commonly form 1-6% of the ordinary RFCC feedstocks, which some half of it turns into coke during the process [1]. Residua include refractory components such as polycyclic aromatic hydrocarbons (PAHs) and heteroatomic compounds. Vacuum gas oil (VGO) as the main feedstock of FCC and RFCC units also comprises portions of such species [2]. Such components have strong adsorption ability on acid sites of catalyst but little reactivity, and so leading to extra coking and suppression of desired products [3].

Coke blocks the micro- and mesoporosity of FCC catalysts and covers the accessible reaction sites [4]. This situation not only results in activity fall and the need in more catalyst make-up [1,2], but also changes the products distribution towards heavy products and gases [5]. Extra coking also leads to excess heat generation in the regenerator, which in turn causes operational fault and increases the riser temperature [1,2,6]. Thus, introducing catalysts with less coke production and controlling the products distribution seems to be crucial for development of RFCC units.

The catalysts of FCC units are essentially formed as microspheres with an average size of 70 μm [1,2]. Y zeolite is the main active catalytic phase of FCC catalysts and comprises a crystalline structure. Although the acid sites of Y zeolite are responsible for most selective catalytic cracking reactions, the population and arrangement of these acid sites because of crystalline structure, causes them to show high affinity for developing hydrogen transfer, cyclization and polymerization mechanisms, which cause severe coking [4,7]. Activity of Y zeolite falls rapidly due to blockage of its micropores of 7.4 Å windows, via coke buildup [5]. All todays' FCC catalysts contain a secondary moderate active phase of generally amorphous silica-alumina matrix [1,2]. The meso- and macroporosity caused by the active matrix, inert filler and binder offer suitable diffusion pathways for feed species especially those of large size, i.e., 1.2-15 nm, which are not admitted to the pores of Y zeolite [8]. The acid sites of matrix are less populated and strong than those of Y zeolite, so matrix shows less activity and coking [6,8,9]. The bimolecular hydrogen transfer reactions which are suspicious for initiating coke production, are highly dependent on the density of acid sites, since hydrogen atoms should be transferred between the molecules adsorbed on adjacent sites [10,11]. Therefore, matrix has less tendency for coke production than Y zeolite, especially from bulky or unsaturated molecules. The active matrix of FCC catalysts also accounts for preliminary cracking (pre-cracking) of the feed components and large molecules. The intermediate products can be cracked on zeolite acid sites (deep-cracking). The balance between the activities of Y zeolite and matrix has been expressed as crucial in adjusting the products of the process [6,8,12].

In conventional FCC catalysts, pre-cracking and deep-cracking occur simultaneously on acid sites of matrix and Y zeolite or both; while it seems that the protection of Y zeolite phase with matrix and imposing pre-cracking/deep-cracking reactions instead can enhance

†To whom correspondence should be addressed.
E-mail: khodadad@ut.ac.ir

the performance of the catalyst [13-16]. Active matrix also serves as a trap for heteroatomic compounds [1,2]. Metallic poisons, which cause irreversible zeolite framework destruction and dehydrogenation mechanisms, are proven to have high mobility in reaction conditions and can penetrate deep inside of the catalyst microsphere [17]. So, pre-cracking reactions and zeolite protection need the matrix layer with comparable thickness to the radius of FCC catalyst particles. We have previously showed that placing a bed of amorphous silica-alumina (ASA) in the upstream of Y zeolite bed instead of a bed of mixed catalysts can enhance the selectivity of deep-cracking products and reduce coking in catalytic cracking of 1,3,5-triisopropylbenzene (TiPB) [13].

TiPB has widely been used as model feed in FCC and RFCC laboratory studies. Its relatively large kinetic diameter (9.4 Å), aromatic ring and alkyl branches are suitable features for representation of species in residual feeds [5,13,16,18-23]. Naphthalene as the simplest form of polycyclic aromatic hydrocarbons (PAHs) has frequently been used in the study of PAHs behavior in catalytic cracking experiments [10,24,25]. Only the 2-ring PAHs can form up to 12 wt% of VGO [2]; they are more resistant to cracking and can be assumed refractory coke producing species [10].

In this study, we represent the idea of bilayer RFCC catalyst particles. Each particle acts as a micro reactor with a top silica-alumina layer for pre-cracking of large molecules and a core Y zeolite part for deep-cracking of the intermediates. The idea is studied by simply applying layers of Y zeolite and silica-alumina on the walls of inert monolith supports, while keeping the total thickness of catalytic layer identical to the radius of FCC catalyst particles. The activities, selectivities and coking of the bilayer catalysts are compared with those of the conventional catalyst of mixed Y zeolite and silica-alumina in catalytic cracking of a model feed composed of TiPB and naphthalene.

EXPERIMENTAL

1. Synthesis of Y Zeolite and Amorphous Silica-alumina (ASA)

Na-Y zeolite (Si/Al of 2.54) was synthesized based on the reported procedures [18]. In brief, proper amounts of sodium aluminate (Riedel-de Haën, technical grade) and sodium hydroxide (Merck) were dissolved in deionized water, followed by dropwise addition of sodium silicate solution (Merck, $SiO_2/Na_2O \approx 3.38$) under vigorous stirring. This resulted in a highly alkaline clear solution. The above solution turned into a transparent gel after 24 h aging in a Teflon autoclave at room temperature. Known amounts of the as-prepared seed gel was added to a solution prepared in the above procedure but with different amounts. The final gel with the molar composition of $4.62Na_2O : 1Al_2O_3 : 10SiO_2 : 180H_2O$ was poured in a Teflon-lined steel autoclave and aged at room temperature for 24 h. Hydrothermal crystallization was carried out at 100 °C for 6 h. The product was thoroughly washed with deionized water and centrifuged to reach the neutral pH, and then dried at 120 °C for 3 h.

Amorphous silica-alumina (ASA) with 13 wt% Al_2O_3 is amongst the most practiced matrices for FCC catalysts [26]. Nano-size amorphous silica-alumina (13 wt% Al_2O_3) was synthesized via co-precipitation method [13]. Diluted sodium silicate solution (Merck, $SiO_2/Na_2O \approx 3.38$) was added dropwise to HCl-acidic solution of aluminum sulfate ($Al_2(SO4)_3 \cdot 18H_2O$ Merck) under vigorous stirring. The vessel was kept in an ice-water bath during the synthesis. The as-prepared gel was poured in a plastic dish and aged at room temperature for 72 h. The product was then ground and washed with deionized water and finally dried at 120 °C for 3 h.

Na-Y zeolite and ASA were ion exchanged, respectively, using 1.5 and 0.5 M solutions of ammonium nitrate (Merck) at 80 °C for 3 h under reflux conditions. 100 ml of NH_4NO_3 solution was used for 10 g of each sample. The product was then washed with deionized water and centrifuged. The ion exchange procedure was repeated three times. The final ammonium-form material was dried at 120 °C for 3 h.

2. Catalysts Preparation

1 cm-long cordierite monolith pieces of 32 channels were cut from a whole body (400 cpsi, 0.18 mm average wall thickness), and used as inert supports for the catalysts. Before coating with the catalysts, the monolith supports were washed, cleaned in an ultrasonic bath, dried at 120 °C and accurately weighted. The catalysts were prepared by (i) coating of Y zeolite and then ASA for bilayer configuration (Y/ASA) and (ii) mixture of Y zeolite and ASA for mixed configuration (Y+ASA) on the walls of monolith pieces (Fig. 1).

Catalytic layers were coated on the monolith supports via dip-coating method [27-29]. Dipping was done in water slurries of 20 wt% solids for 30 s. 5 wt% of the solid content was SiO_2 binder of Ludox AS-40 colloidal silica (Aldrich, 40 wt%). The excess liquid was gently removed by blowing air followed by flushing with pressurized air to throw out weakly adhering parts. The support was then placed in warm blowing air at 60 °C. Desired amounts of catalysts were coated on the supports by repeating the coating procedure. The total weights of the coatings (0.1±0.0005 g) were adjusted to result in a layer thickness comparable to the FCC catalyst particles of 35 μm radius. Y zeolite and ASA contents of both configurations were also identical.

To evaluate the catalytic activities of the individual catalyst constituents, NH_4-Y zeolite and ammonium exchanged ASA were also

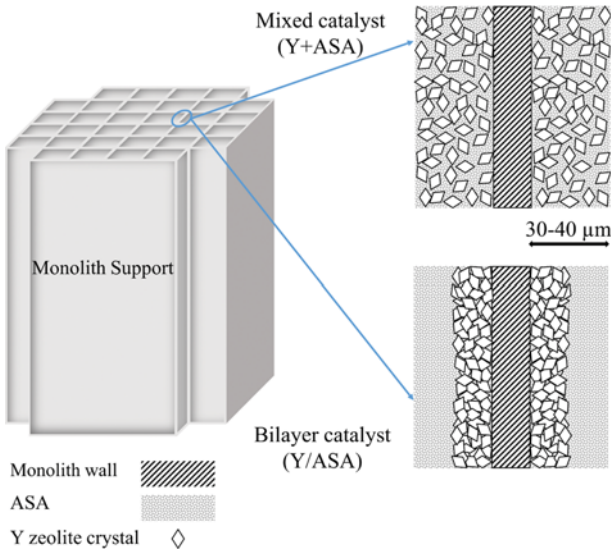

Fig. 1. Illustrations of the mixed (Y+ASA) and bilayer (Y/ASA) catalyst configurations prepared on monolith supports.

coated on the monolith supports and tested in catalytic cracking experiments. SiO_2 binder showed no significant acidity and cracking activity (not presented here).

3. Catalyst Characterization

X-ray diffraction (XRD) patterns of NH_4-Y zeolite, HY zeolite (after 5 h calcination at 550 °C) and ASA were obtained by using a Rigaku X-ray diffractometer with radiation of Cu Kα (λ=1.5406 Å), working at 40 kV, 40 mA. The scanning was done in the 2θ range of 5-50 with a step size of 0.02 degree. The XRD pattern of NH_4-Y zeolite was compared to the standard pattern of Na-Y zeolite reported in ASTM D3906. Reflections of (511), (440), (533) and (555) peaks were used to estimate relative crystallinity (RC) and unit cell size (USC) of the samples according to ASTM D3906 and ASTM D3942 standards, respectively. Si/Al atomic ratio was calculated from Si/Al=(192-N_{Al})/N_{Al} were N_{Al} is the number of aluminum atoms per unit cell, based on a published formula in [30]. Scherrer's equation was applied on the aforementioned reflection peaks for estimation of approximate crystallite size.

BET surface areas and pore size distributions (PSD) of the samples were evaluated using a Micromeritics TriStar II ASAP apparatus. The N_2 adsorption-desorption isotherms were measured at liquid nitrogen temperature for the full range of N_2/He relative pressures. The samples were degassed at 300 °C for 3 h before the measurements.

Temperature programmed desorption of ammonia (NH_3-TPD) was conducted using a Quantachrome CHEMBET-3000 apparatus. 0.1 g of the sample was in-situ activated for 1.5 h at 500 °C under nitrogen to give protonated catalyst by releasing ammonia [31]. Adsorption of ammonia was for 15 min at 100 °C using a stream of 5 vol% of anhydrous ammonia in helium. The system was purged under helium at the same temperature for 30 minutes. NH_3-TPD was performed by heating the sample from 100 °C to 600 °C (10 °C/min) under helium flow, while monitoring the effluents. After each TPD experiment, 0.5 ml of anhydrous ammonia was injected to the helium stream for calibration of the TCD signal.

The morphological and structural characteristics of the synthesized samples were studied using field emission scanning electron microscopy (FE-SEM) by a MIRA3 TESCAN (15KV) microscope. In the case of cross-section imaging, the samples were polished by sandpaper to 5 μm roughness. In the case of imaging the morphologies of catalyst layers, the samples were broken to give a higher resolution of the cross-section.

4. Catalytic Cracking Experiments

Catalytic cracking tests were done in a laboratory set-up schematically shown in Fig. 2. The feed was composed of 90 wt% 1,3,5-triisopropylbenzene (95%, Aldrich) and 10 wt% naphthalene (99%, Aldrich). The liquid hydrocarbon feed was injected by a syringe pump (Atom 1235N, Japan) into a 1/16" steel pipe directed into the hot zone of the reactor. The feed was diluted with argon to 5 vol%. To minimize the dead volume above the catalyst bed, a portion of argon flow was fed from the top of the reactor via a mass flow controller (MFC- UNIT8100). The reactor was a quartz tube of 1 cm ID and 15 cm length. The temperature of the reactor was controlled using a PID temperature controller (Digi-Sense R/S). Temperature sensing was done with a J-type thermocouple placed inside the catalyst bed. About 3 cm above the catalyst bed was packed with

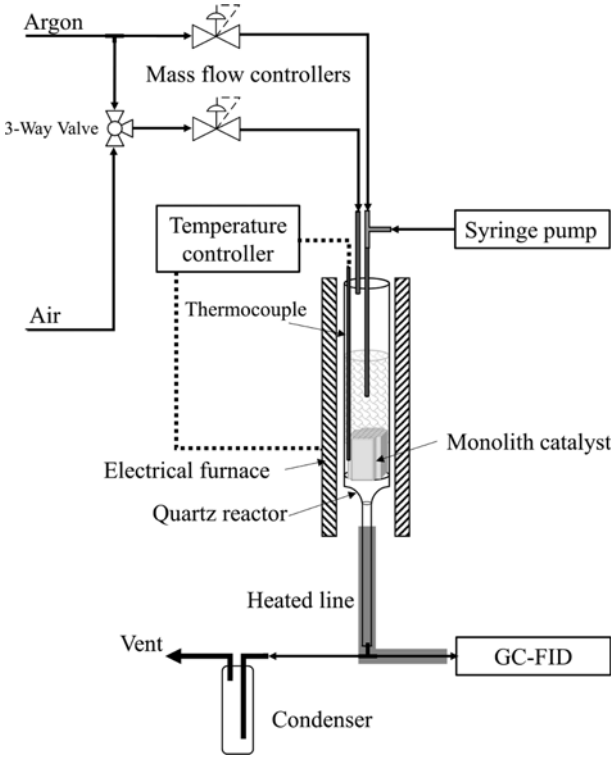

Fig. 2. Laboratory set-up used for catalytic cracking experiments.

quartz grains of 18-40 mesh size for enhancement of the feed evaporation and distribution. Fine quartz grains of 50-200 mesh size were used to fill the gap between the monoliths and the reactor wall to eliminate by-pass flow. The reactor effluent was split and a portion of 20 ml/min was sent to a GC analyzer (PerkinElmer 8410) through a 1/8" pipe, temperature of which was kept at 175 °C to assure no condensation. The GC analyzer was equipped with an FID detector and a 1.5 m, 2.2 mm ID column packed with SE-30, 25% on Chromosorb P.

Catalytic cracking experiments were done on Y zeolite, ASA, bilayer (Y/ASA) and mixed (Y+ASA) catalysts at 300, 350 and 400 °C reaction temperatures. Higher temperatures were avoided, due to the significant thermal cracking of TiPB starting at 375 °C [13]. Prior to the catalytic cracking reactions, the catalysts were in-situ activated at 500 °C under 20 SCCM flow of air for 1 h. The liquid feed was injected with a flow of 20 ml·$g_{catalyst}^{-1}$ h^{-1}. The reactor effluents were analyzed on the online GC at 0.5, 8 and 16 minute times on stream (TOS). The coke on the catalysts was evaluated at two TOS, one on catalysts after 140 s of catalytic cracking and the other after 980 s, which respectively represent the state of the catalysts at the beginning of the reaction and the deactivated state of the catalysts at increased reaction time.

5. Temperature Programmed Oxidation (TPO) of Coked Catalysts

The coke content of the catalysts after the catalytic cracking experiments was evaluated in the same set-up shown in Fig. 2, which was modified for the TPO experiments. The catalysts were placed in the tubular quartz reactor and the temperature was raised to 900 °C at 10 °C/min under 50 SCCM flow of 2.5% O_2 in helium.

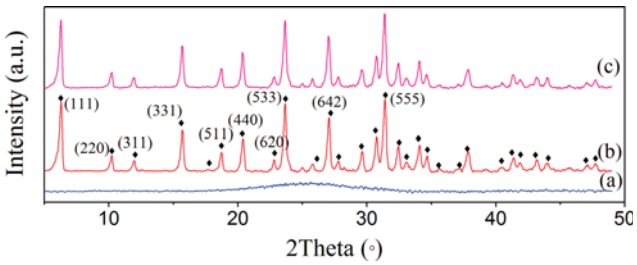

Fig. 3. XRD patterns of synthesized samples, (a) ASA, (b) NH_4-Y, (c) HY and (◆) ASTM D3906 standard pattern of Na-Y zeolite.

A lean oxygen flow was used to mimic incomplete combustion in dense catalyst regions of RFCC regenerator [1]. The effluent gases were analyzed every minute with an FTIR spectrometer (Bruker vector22) equipped with a gas cell of 2 cm ID and 10 cm length and windows of NaCl. FTIR analyses were done at transmittance mode and resolution of 5 cm^{-1} in the range of 4,000 cm^{-1} to 400 cm^{-1}. The areas under peaks in the range of 2,400-2,280 cm^{-1} and 2,235-2,030 cm^{-1} were used for CO_2 and CO analyses, respectively. For evaluation of quantitative amounts, the FTIR response was calibrated for CO_2 and CO with respectively 5,000 and 1,000 ppm of the gas in air.

RESULTS AND DISCUSSION

1. Characterizations

XRD patterns of the synthesized NH_4-Y zeolite and HY zeolite after calcination at 550 °C, along with the peak positions of standard XRD pattern of Na-Y zeolite based on ASTM D3906 are presented in Fig. 3. The XRD pattern of NH_4-Y zeolite shows good agreement with the standard pattern. Y zeolite has retained its crystalline structure in exposure to the calcination temperature, confirming its thermal stability in the range of the catalytic cracking temperatures. Table 1 summarizes the BET surface areas of the samples and their characteristic data derived from the XRD patterns. UCS, number of Al atoms per unit cell and the atomic ratio of Si/Al of the HY zeolite were calculated to be 24.74 Å, 54 and 2.54, respectively. The attained Si/Al ratio of the Y zeolite lies in the typical range for use in FCC catalysts [2].

Table 1. Characteristics of the synthesized samples

Sample	BET surface area ($m^2 \cdot g^{-1}$)	RC[a] (%)	UCS[b] (Å)	Si/Al	Crystallite size (nm)
ASA	343	-	-	-	-
NH_4-Y	779	100	24.77	2.37	430
HY	771	98	24.74	2.54	Not calculated

[a]Relative crystallinity
[b]Unit cell size

Relative crystallinity (RC) of Y zeolite shows only 2% decrease after calcination. The higher Si/Al ratio of HY zeolite and its smaller UCS than those of NH_4-Y zeolite can be attributed to partial dealumination of Y zeolite [18] in high temperature treatments. The decrease in the BET surface area of Y zeolite after calcination is also in line with the loss of crystallinity and decrease in UCS.

Fig. 4(a), shows the FE-SEM micrograph of polyhedral crystals of NH_4-Y zeolite with an approximate average size of 1 μm. This indicates agglomeration of two or three crystallites, when compared to the crystallite size of 430 nm derived from Scherrer's equation (Table 1). The crystal size of the synthesized Y zeolite lies in the preferred range for use in RFCC catalysts. Small crystals of zeolite are reported to have positive impacts on catalytic activity and selectivity towards light intermediates [32,33].

XRD pattern of ASA (Fig. 3) indicates its amorphous structure. The FE-SEM micrograph of ASA is also provided in Fig. 4(b). BET surface area of ASA was determined to be 343 m^2/g (Table 1). This can be used for a rough estimation of ASA average BET particle size (d_{BET}). Assuming the spherical grains of silica-alumina, d_{BET} was calculated to be about 5 nm. N_2 adsorption-desorption isotherms of the samples and the PSD plots were used to study the pore structures of the samples (Fig. S1, supplementary material). The synthesized Y zeolite is a microporous material with narrow pore size

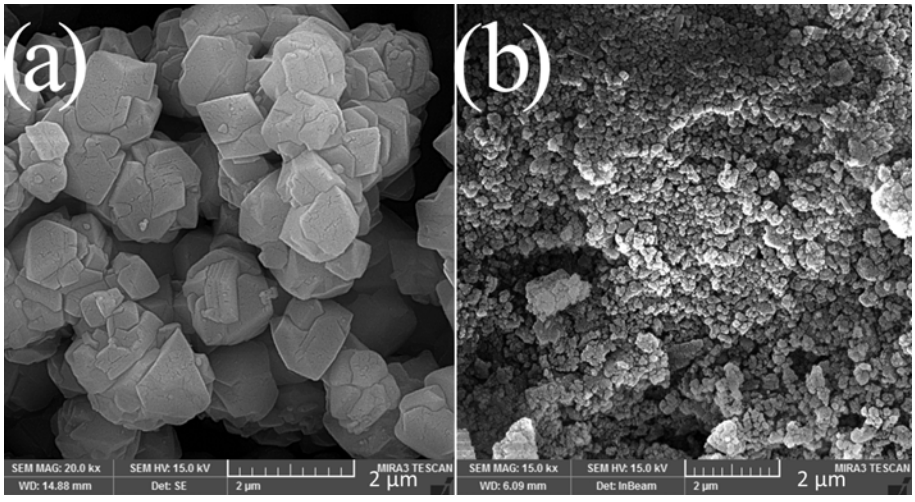

Fig. 4. FE-SEM images of (a) Y zeolite, and (b) ASA.

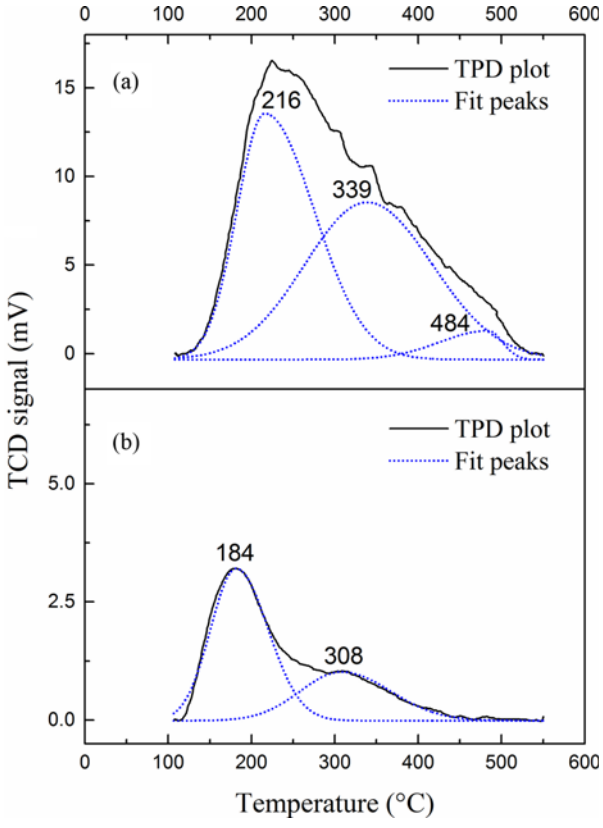

Fig. 5. NH_3-TPD plots of (a) Y zeolite and (b) ASA, along with the deconvoluted peaks.

distribution. The main porosity of Y zeolite belongs to the pores of about 1.4 nm diameter close to the size of Y zeolite supercage. ASA has a mesoporous structure with a wide pore size distribution in the range of 2-100 nm, with a peak at about 4 nm pore diameter. The mesoporosity of ASA as the matrix of RFCC catalyst, offers suitable pathways and reaction sites for feed molecules.

Fig. 5 shows the NH3-TPD plots of synthesized Y zeolite and ASA along with the deconvoluted curves according to Gaussian method. Although NH_3-TPD technique is unable to distinguish between Brönsted and Lewis acidity, it is a widely accepted method to estimate the amount and strength of acid sites by measuring desorbed ammonia as a basic probe molecule [19]. NH_3-TPD plot of Y zeolite shows three main peaks around 220 °C, 340 °C and above 450 °C which are, respectively, attributed to weak, medium and strong acid sites [13,19].

Total acidity and the proportions of different acid site strengths were calculated from TPD plots and reported in terms of the amounts of desorbed ammonia for both samples (Table S1, supplementary material). Y zeolite shows about eight-times higher total acidity than ASA. ASA ammonia TPD profile (Fig. 5(b)) shows no significant peak above 400 °C, implying the lack of strong acidity. Weak acidity forms approximately 47% and 67% of total acidity in Y zeolite and ASA, respectively. The weak acidity is ascribed to weak Lewis and Brönsted acid sites, terminal Si-OH groups, and adsorbed ammonia on non-acidic sites [19]. Medium acidity forms higher portion of the total acidity for Y zeolite compared to ASA. Weak and medium acidity peaks in ASA TPD plots appear at relatively lower temperatures than those of Y zeolite (Fig. 5), implying less

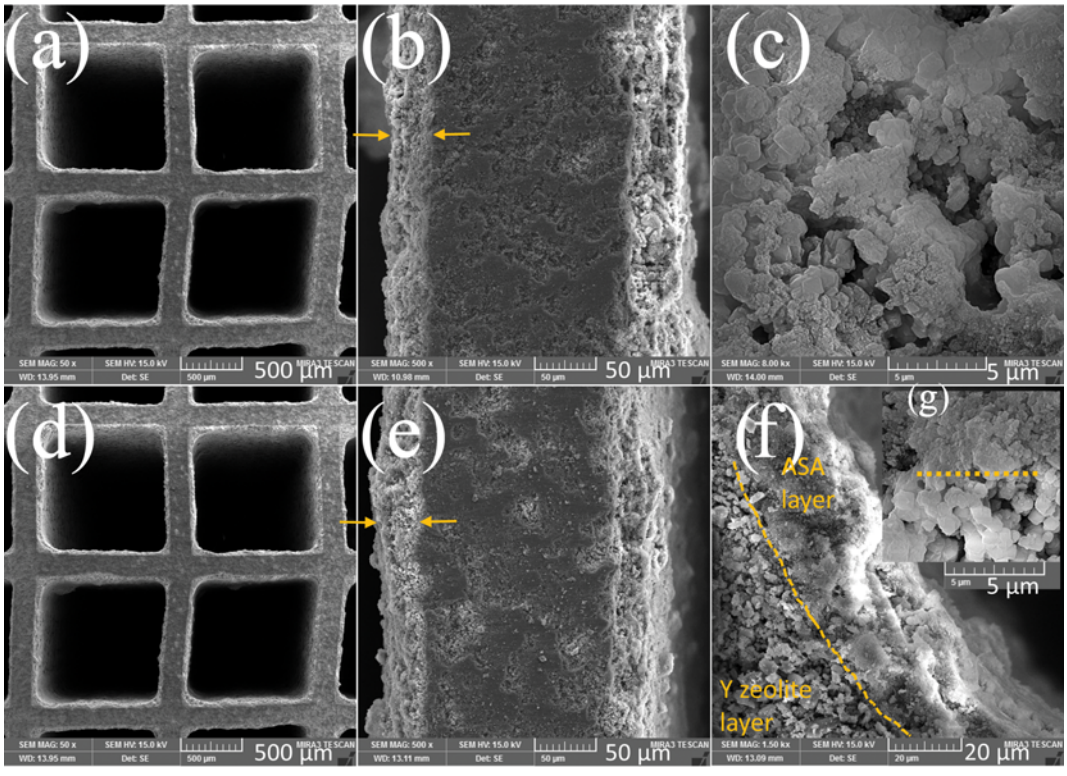

Fig. 6. FE-SEM images of, (a), (b), (c) the mixed catalyst (Y+ASA) and (d), (e), (f) the bilayer catalyst (Y/ASA) in different magnifications, (g) the interface of Y zeolite and ASA layers in Y/ASA catalyst.

strong nature of these sites in the former. Brönsted acid sites in ASA are hydroxyl groups coordinated with trigonal aluminum atoms and can be converted to Lewis acid sites by dehydration at high temperatures. The nature of acid sites of zeolites is somehow different. Brönsted acid sites of zeolites are generally formed by ion exchange with NH_4^+ followed by thermal decomposition of ammonium ions to give protons which counterbalance the negative charge of the network. Lewis acid sites of zeolites belong to extra-framework and structural Al atoms of the network [34]. Acid strength in zeolites is highly affected by crystalline structure and increases by decrease in the number of Al atoms in next nearest neighbor coordination of structural aluminums [13].

2. The Structures of the Bilayer and Mixed Catalysts

The FE-SEM images of mixed (Y+ASA) and bilayer (Y/ASA) catalysts are presented in Fig. 6. Both samples show uniform and complete coverage of support walls by catalyst layers (Fig. 6(a) and (d)). The layer thicknesses for both configurations were adjusted approximately to 35 μm (Fig. 6(b) and (e)) close to the average radius of conventional FCC catalysts. This was achieved by repeated cycles of dip-coating and drying. Fig. 6(c) shows the morphology of the catalytic layer of mixed catalyst. Co-existence of both crystalline Y zeolite and amorphous matrix is shown in the figure, which resembles the locations of catalyst constituents in conventional FCC catalysts. In the case of bilayer configuration, the hierarchical layout of the catalyst constituents is clearly shown in Fig. 6(f). The bilayer catalyst comprises a layer of Y zeolite crystals of about 20 μm thickness, which is protected with a top layer of ASA while keeping the total layer thickness and the catalyst weight the same as those of the mixed catalyst. Fig. 6(g), shows higher magnification of the interface of the two layers in the bilayer catalyst.

3. The Catalytic Activities and Products Distributions

3-1. Low Time on Stream

The yield was defined as the molar flow rate of a product per the molar flow rate of converted feed. The flow rate of propylene was divided by 3. Molar yields of products and the feed conversions in catalytic cracking experiments at 350 °C and 30 second time on stream (TOS) are shown in Fig. 7. In industrial FCC applications, the catalysts are separated from the products after a few seconds of traveling in the reactor riser and sent to the regenerator. All major catalytic cracking reactions occur in a few seconds before catalyst deactivation [1,2]. Study of the catalysts at the beginning stages of reaction may bring a practical insight into their activity. Regarding Fig. 7(a), Y/ASA shows the highest propylene yield amongst the catalysts. Propylene is produced in all successive dealkylation reactions of TiPB and its major derivatives and can be assumed as an indicator of catalyst activity, though it can also be converted to coke [35]. ASA with the lowest amounts of total acidity shows the least activity for TiPB cracking, and even lower for naphthalene (Fig. 7(a)). Although Y zeolite comprises more total and strong acidity than Y+ASA and Y/ASA that only have 50% Y zeolite, the two latters show higher cracking activity, more benzene and less cumene and DiPBs production. Conversions of TiPB and naphthalene are slightly higher for Y/ASA than Y+ASA (Fig. 7(a)). The yield of benzene as the main deep-cracking product increases in the order of ASA (5%)<Y zeolite (27%)<Y+ASA (52%)<Y/ASA (69%). The situation is vice versa in the case of heavy products (DiPBs), such that the selectivity of benzene to DiBPs ($S_{benz/DiPB}$) is 33.6, 10.4, 1.4, 0.15 for Y/ASA, Y+ASA, Y zeolite and ASA, respectively (Fig. 7(a)). This indicates that the bilayer configuration has excelled in deep-cracking of the feed and heavy products.

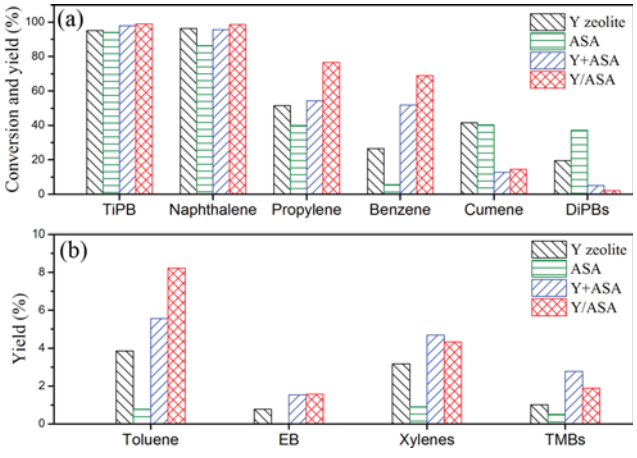

Fig. 7. The feed conversions and the yields of products for reaction at 350 °C and time on stream of 30 s, (a) major products, and (b) by-products.

Crackability of propyl-benzenes was reported to decrease in the order of TiPB>DiPBs>cumene [20]. TiPB which is not admitted into the micropores of Y zeolite would be readily cracked on weak acid sites of ASA or surface acid sites of Y zeolite crystals and gives 1,3 DiPB and propylene [31]. Although dealkylation of 1,3 DiPB needs more strong acidity to proceed, it could already be cracked on ASA to high extent to produce cumene. On Y zeolite crystals, 1,3 DiPB of 8.4 Å size [16] is either dealkylated on surface acid sites or isomerized to 1,4 DiPB, which can enter the Y zeolite microporosity of 0.74 Å and produce cumene [23]. Cumene thus is the major product for both ASA and Y zeolite (Fig. 7(a)). Dealkylation of cumene to benzene is supposed to occur only on strong Brönsted Acid sites [36], so benzene forms only a negligible amount of the products on ASA which lacks enough strong acidity (see Fig. 5).

Higher activities and more yields of deep-cracking products on Y/ASA and Y+ASA than those on Y zeolite are attributed to more coking tendency of the latter. Coke deposits on acid sites, covers the accessible catalyst surface and blocks the microporosity of Y zeolite crystals and hinders further deep-cracking of cumene and DiPB. Incorporation of ASA in catalysts provides accessibility to catalytic sites [22] and partially pre-cracks TiPB to produce less bulky intermediates of DiPB and cumene, which can be deep-cracked on zeolite acid sites. The superiority of Y/ASA in cracking activity and selectivity toward deep-cracking products, compared to Y+ASA is ascribed to two-stage reactions of pre-cracking and deep-cracking stemming from unconventional location of Y zeolite and ASA (see Fig. 6) in the bilayer catalyst. TiPB is precracked to DiPB and cumene on the ASA top layer of the bilayer catalyst. The products of precracking then undergo deep-cracking on the zeolite underneath layer. This leads to less contact of zeolite selective sites by bulky and coke producing species. This in turn causes higher catalytic activity and selectivity toward light products in the bilayer catalyst. The direct contact of feed molecules with zeolite acid sites

in the conventional Y+ASA catalyst leads to more coke buildup on zeolite crystals that decreases deep-cracking of intermediates to light products.

Naphthalene with a planar molecular structure, big size and two aromatic rings is more likely to be adsorbed on acidic sites of catalyst and initiate coking rather than cracking. However, some reports show that PAHs can be partially cracked to give benzene or other derivatives [10,24]. PAHs are supposed to be strong coke precursors in catalytic cracking reactions [3]. These compounds can severely attack the proton sites of Y zeolite due to rich electron sources of the aromatic rings [24]. High density of acid sites in Y zeolite favors the adsorption of naphthalene on nearby sites and prompting hydrogen transfer reactions [10]. Its contact with Y zeolite may cause suppression of deep-cracking by covering the selective acid sites, while the acid sites of ASA are of no importance in production of benzene. The deposition of some portions of naphthalene on ASA top layer shows a significant impact in development of deep-cracking reactions and benzene production in Y/ASA catalyst.

Although the major products of TiPB catalytic cracking are produced by successive propylene abstractions, minor species of toluene, ethylbenzene (EB), xylenes and trimethybenzenes (TMBs) are also produced by transalkylation, isomerization, disproportionation and other secondary reactions [21,23,25,37]. Fig. 7(b) shows the yields of these minor by-products. ASA shows the least, nearly none, and Y/ASA shows the highest yields of these products. Production of such by-products not only requires strong acidity for production of methyl and ethyl groups via propylene cracking or TiPB and DiPB side-chain cracking, but also requires special geometry of acid sites [23]. Shape selectivity is also considered in production of isomers over zeolite catalysts [37,38]. These secondary reactions need simultaneous adsorption of molecules on multiple acid sites, compared to monomolecular catalytic cracking reactions [2]. It seems that the acid sites inside Y zeolite pores play a dominant role in proceeding of the secondary reactions. In this regard, the bilayer catalyst yields higher amounts of these species, especially toluene, than the mixed catalyst. This is attributed to less zeolite pore plugging and more accessibility to acid sites of zeolite crystals in the bilayer catalyst. Indeed, pre-cracking of feed molecules in ASA layer and less contact of heavy species with Y zeolite in Y/ASA compared to Y+ASA conserve more active zeolite sites for selective reactions. Thus, toluene with the yield of 8% forms a notable portion of the bilayer catalyst products.

3-2. The Effect of Reaction Time

Fig. 8 shows the feed conversions for the catalysts during 16 minutes of catalytic cracking at 350 °C. As shown in Fig. 8(a), ASA shows the highest deactivation amongst the studied catalysts, due to its low acidity. The acid sites of ASA are not enough in both number and strength to crack all the incoming feed at high TOS and are deactivated soon via coke formation. The same situation can be seen for naphthalene conversion, regarding Fig. 8(b).

The excessive deactivation of ASA starts after 8 min TOS, before which ASA is deactivated in the same trend as Y zeolite (Fig. 8(a) and (b)). The yields of the major products in Fig. 9 also show sharp changes around the point of 8 min TOS. In Fig. 9(b) and d, which, respectively, show the yields of benzene and DiPBs, the bilayer catalyst shows better performance than the mixed catalyst in deep-

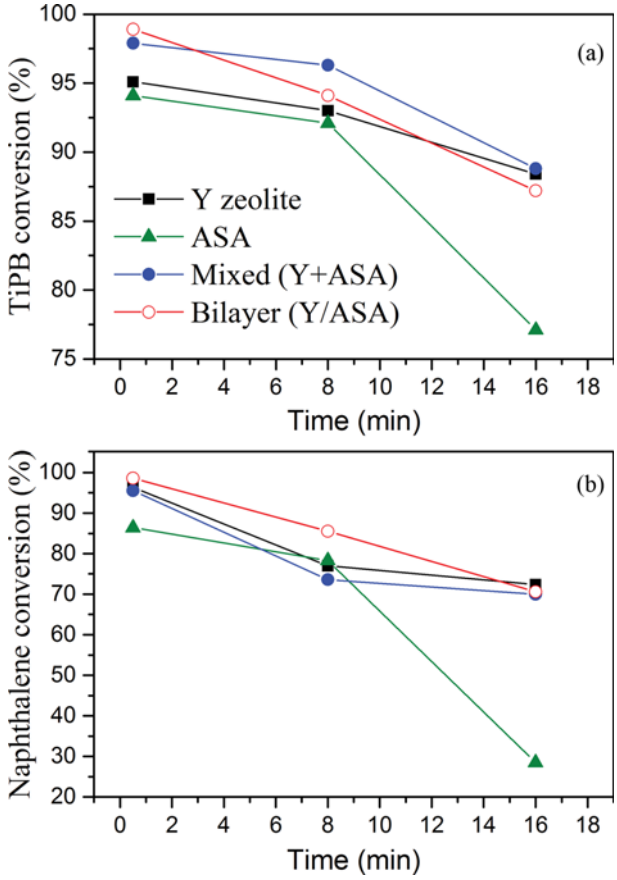

Fig. 8. Conversion of TiPB (a) and naphthalene (b) during 16 min catalytic cracking at 350 °C, for Y zeolite (■), ASA (▲), Y+ASA (●) and Y/ASA (○) catalysts.

cracking and reducing the heavy products before 8 min TOS. At the same time span, propylene production is also higher for Y/ASA than Y+ASA (Fig. 9(a)). This indicates more successive catalytic cracking reactions on the bilayer catalyst. As discussed in section 3.1, the ASA top layer of Y/ASA precracks the feed molecules, and the intermediate products are then deep-cracked on Y zeolite layer. ASA layer also serves as a trap for naphthalene molecules and protects the selective acid sites of the underneath Y zeolite layer. At increased TOS, ASA starts to be deactivated much faster than Y zeolite (Fig. 8(a) and (b)). Since deactivation and coke buildup proceed from the outer surface towards the center of the catalyst particles [39], the bilayer catalyst loses its superiority over the mixed catalyst at increased TOS (Fig. 9(b) and (d)), due to deactivation of the protective top layer. However, the mixed catalyst may still take advantage of some ASA content deep inside the catalytic layer not fully deactivated. This is, however, not a deficiency of the bilayer catalyst, since in FCC industry the catalysts are separated after a few seconds of catalytic cracking and sent to the regenerator [1,2].

Cumene is an intermediate product which results from the cracking of DiPBs and can be cracked to give benzene and propylene. Regarding Fig. 9(c), the least cumene yield for Y zeolite, Y+ASA and Y/ASA can be seen at the beginning of the reaction. By increasing the reaction time, the strong acid sites of zeolite responsible for cumene cracking [23,36] are deactivated via coke buildup, while

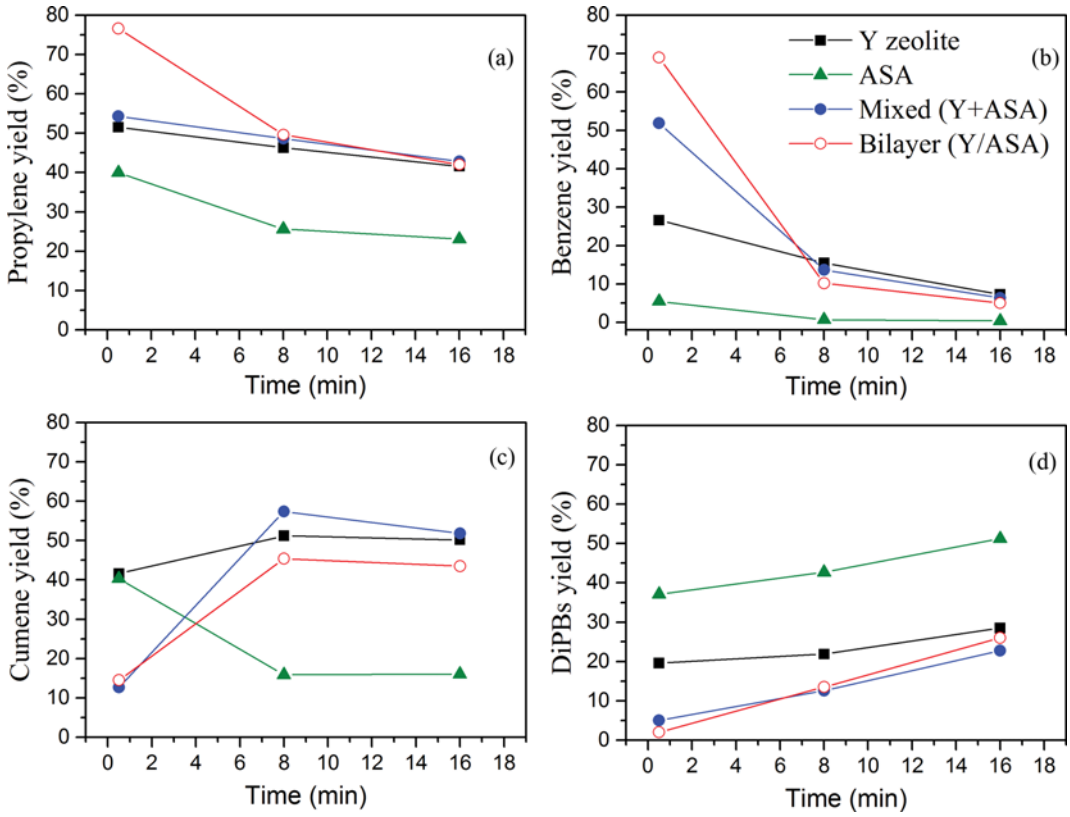

Fig. 9. The yields of propylene (a), benzene (b), cumene (c) and DiPBs (d) during 16 min catalytic cracking at 350 °C, for Y zeolite (■), ASA (▲), Y+ASA (●) and Y/ASA (○) catalysts.

there is still enough acidity to convert DiPBs to cumene. This results in a rise in the cumene yield at the shorter TOS. In this region, both Y+ASA and Y/ASA catalysts yield less cumene and more benzene than Y zeolite (Fig. 9(c) and (b)), due to the precracking function of ASA. In addition, Y/ASA shows even less cumene production and more benzene and propylene yields than Y+ASA (Fig. 9(c), (b) and (a)). This confirms that ASA top layer in the bilayer catalyst can conserve the underneath zeolite layer from excessive coking, leading to more deep-cracking reactions on strong acid sites of zeolite.

4. Coke Evaluation

CO_2 and CO evolution during temperature programmed oxidation of coked catalysts are illustrated in Fig. 10 for catalysts after 140 s time on stream in catalytic cracking at 350 °C. The cumulative results calculated from the areas of TPO plots are presented in Table 2. The carbon content of the catalysts was calculated from the total amounts of CO_2 and CO and was evaluated to be 16.8, 10.1, 8.3 and 1.8 wt% for Y zeolite, Y+ASA, Y/ASA and ASA, respectively (Table 2). High coke yield of Y zeolite is a result of its high total acidity. Populated acid sites can adsorb hydrocarbons nearby and undergo hydrogen transfer, cyclization and polymerization mechanisms [10,11]. The less coke content of the bilayer and the mixed catalysts, compared to Y zeolite, is on one hand due to less total acidity and on the other hand the result of precracking role of ASA. The bilayer catalyst produces even 18% less coke than the mixed catalyst. As discussed in the previous section, the superiority of the bilayer catalyst in coke suppression and light products selectivity is

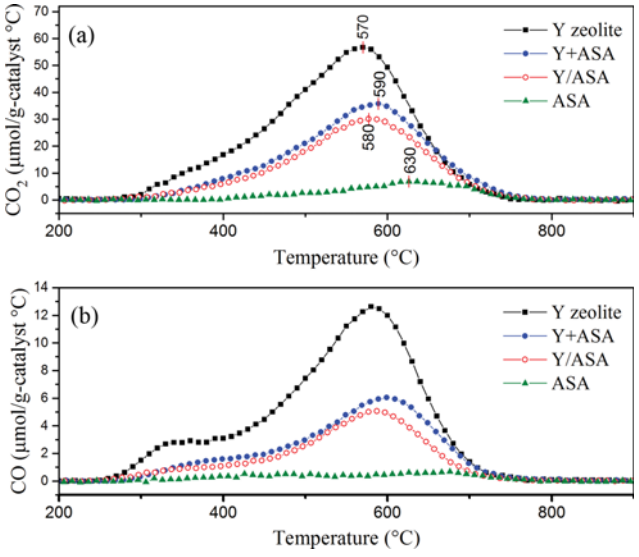

Fig. 10. CO_2 (a) and CO (b) evolution during TPO of the cokes on the catalysts after reaction at 350 °C and time of stream of 140 s.

ascribed to two-stage reactions of pre-cracking/deep-cracking. The feed molecules and heavy products are allowed to undergo pre-cracking reactions in ASA top layer. This results in less bulky intermediate products. The intermediate products then can be deep-cracked on selective acid sites of the zeolite. However, in the case

Table 2. Cumulative results of the temperature programmed oxidation of the coked catalysts for reaction at 350 °C and time on stream of 140 s

Catalysts	Y zeolite	ASA	Y+ASA	Y/ASA
CO_2 evolution (mmol/g-catalyst)	11.47	1.31	7.18	5.97
CO evolution (mmol/g-catalyst)	2.51	0.17	1.23	0.97
Carbon content (wt%)	16.8	1.8	10.1	8.3
Molar CO/CO_2	0.22	0.13	0.17	0.16

of conventional mixed catalysts, precracking and deep-cracking reactions occur simultaneously on acid sites of both ASA and zeolite. This results in more contact of heavy and bulky species with the surface of Y zeolite crystals which leads to more coke buildup. On the other hand, naphthalene has high tendency to deposit on populated zeolite acid sites, leading to coverage of active catalytic surface, while ASA top layer of the bilayer catalyst can entrap such molecules and provide a better zeolite protection.

CO may be produced by incomplete combustion of coke in compact catalyst regions of the FCC regenerator, where oxygen supply is not enough for stoichiometric combustion to CO_2. CO production in FCC regenerators should be avoided due to the operational severity and environmental regulations [1,2]. In experimental conditions of this study, CO may be produced in combustion of relatively large coke islands and the coke deposited in micropores where diffusion limitations may exist. The ratio of CO/CO_2 is an indicator of such cokes. Y zeolite shows the highest and ASA the lowest CO/CO_2 ratios (Table 2). Both Y/ASA and Y+ASA show lower values of CO/CO_2 than Y zeolite, while Y/ASA shows even lower CO/CO_2 than Y+ASA. High CO/CO_2 ratio of Y zeolite indicates massive blockage of its microporosity, while the deactivation is less harsh when ASA exerts some degrees of precracking. Protection of zeolite phase with ASA layer in the case of Y/ASA catalyst is responsible for less coke in zeolite microporosity compared to Y+ASA catalyst and less CO production during the regeneration.

Both CO_2 and CO profiles show higher TPO peak temperatures for ASA than Y zeolite (Fig. 10). This indicates the more refractory nature of ASA coke. ASA deactivates faster than the other catalysts, due to lower concentration of acid sites. The produced coke then adsorbs adjacent hydrocarbons and transfers hydrogen with the gas phase molecules [4,10]. It is also predicted that the mesoporosity of ASA provides enough space for cyclization of coke species, which results in reduced H/C and more hard coke [13]. High portions of coke in Y zeolite are, however, confined in microporosity of crystals with less space for growth and accessibility to gas phase hydrocarbons. A relatively low temperature shoulder is also seen in TPO plots of the zeolite containing catalyst, which is more obvious in CO evolution profiles (Fig. 10(b)). The shoulder is attributed to relatively soft or non-catalytic coke adsorbed in the microporosity of zeolite. The noticeable shoulder in Y zeolite TPO profiles, especially in CO evolution one, is in line with high CO/CO_2 ratio. The peaks in TPO profiles of Y/ASA appear at about 10 °C lower temperature compared to Y+ASA. This shows slightly less refractory nature of the coke formed on the bilayer catalyst than that on the mixed one.

Catalysts after 980 s time on stream in catalytic cracking at 350 °C were also subjected to TPO analyses, to study the coke production in excessive catalyst deactivation situation. TPO analyses confirm the influence of the bilayer configuration in reducing the coke content of the catalyst (Fig. S2, supplementary material). The carbon content of the coked catalysts was evaluated to be 38.2, 3.4, 15.8 and 12.4 wt% for Y zeolite, ASA, Y+ASA and Y/ASA, respectively. The bilayer catalyst produces 21% and 67% less coke than the mixed catalyst and Y zeolite, respectively. Comparing these results with those of 140 s TOS (see also Table 2) shows that about 40-60% of the total coke of the catalysts is produced at the early times before extended deactivation. This indicates a decline in coke formation rate by reaction time [40]. The difference of coke content of the bilayer and mixed catalysts is more significant for highly deactivated catalysts after 980 s than that after 140 s time on stream. The study of the coke on the catalysts for both low and high TOSs indicates that the bilayer configuration excels in reducing the amount and severity of coke which may suited for in RFCC applications.

5. The Effect of Reaction Temperature

Effects of the reaction temperature on the performance of the mixed and bilayer catalysts were studied. Fig. 11 along with Fig. 7(a) show the yields of products and the feed conversions for the two catalyst configurations for reaction temperatures of 300, 350 and 400 °C with 30 s time on stream. The selectivity towards benzene increases with reaction temperature for both catalysts, which is in accordance with the other reports [21,23,38]. At 400 °C, benzene becomes the predominant product and only negligible amounts of DiPBs and cumene are produced. Y/ASA shows more benzene selec-

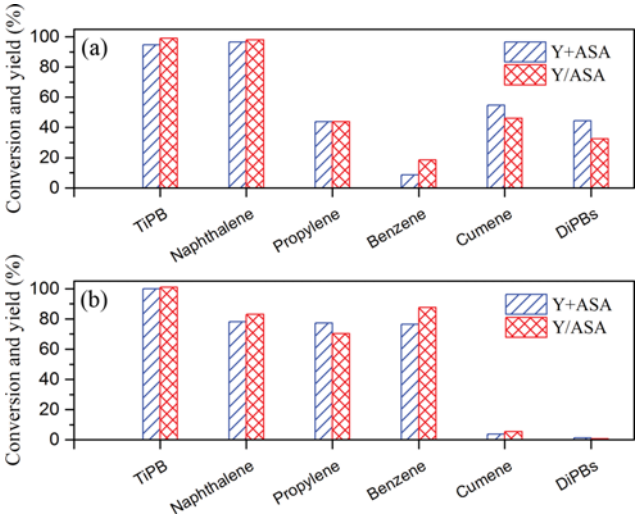

Fig. 11. The feed conversions and the yields of products for (a) 300 °C and (b) 400 °C reaction temperatures and time on stream of 30 s.

tivity than Y+ASA for all temperatures, while the difference decreases by increasing the temperature. Y/ASA yields 113%, 33% and 15% more benzene than Y+ASA for 300, 350 and 400 °C, respectively. The decline is attributed to the increase in thermal cracking of TiPB [13] and the decrease of non-catalytic coke with increasing the reaction temperature. High portions of coke on FCC catalysts are supposed to be non-catalytic cokes or condensed hydrocarbons [4], the amount of which decreases with temperature [40]. The coke, however becomes more refractory and burns at higher temperatures (data are not shown here).

The difference in TiPB conversion for the two catalysts is also vanished at 400 °C. However, at 350 and 300 °C, Y/ASA shows slightly higher TiPB conversion than Y+ASA due to less coking and more accessibility to active sites. Naphthalene conversion considerably decreases by increasing the reaction temperature. This indicates that naphthalene can majorly deposit and condense on acid sites of catalyst rather than cracking, especially at lower reaction temperatures, thus increasing the temperature leads to less conversion of naphthalene.

CONCLUSIONS

A novel bilayer catalyst (Y/ASA) composed of Y zeolite protected by a layer of amorphous silica alumina and a conventional mixed (Y+ASA) catalyst was prepared and compared in catalytic cracking of a model RFCC feed composed of TiPB and naphthalene. The catalytic cracking performance of Y/ASA was significantly better than that of Y+ASA in enhancing the yields of deep-cracking products and suppression of the coke. Y/ASA catalyst produced 33% and 46% more benzene and toluene, respectively, and 18% less coke than Y+ASA catalyst. The coke produced by Y/ASA was also less refractory than that by Y+ASA as burnt at slightly lower temperatures, and its combustion results in less CO emission. We concluded that the hierarchical layout of the catalyst constituents in Y/ASA leads to two-stage reactions of pre-cracking and deep-cracking, respectively, in ASA top layer and Y zeolite underneath layer of the catalyst. Pre-cracking of the feed undergoes to high extents in ASA top layer and the intermediate products are then subjected to deep-cracking on selective acid sites of Y zeolite layer. ASA top layer in Y/ASA also serves as a trap for naphthalene, preventing it from contact with zeolite part of catalyst. On the other hand, direct contact of TiPB and naphthalene with acid sites of Y zeolite in Y+ASA would lead to surface coverage and pore blockage of zeolite crystals by the coke buildup. More accessible catalytic sites of the bilayer catalyst, especially those of Y zeolite intracrystalline acid sites, play a significant role in increasing the selectivity of deep-cracking products. The bilayer configuration of Y zeolite/silica-alumina shows promising features for increasing bottoms cracking and suppressed coking if applied on RFCC catalyst particles.

SUPPORTING INFORMATION

Further results and discussions about N_2 adsorption-desorption isotherms and pore size distributions of Y zeolite and ASA, acidic properties of the samples calculated from TPD plots and the TPO plots of the coked catalysts in long reaction time can be found in "SUPPORTING INFORMATION" section.

Additional information as noted in the text. This information is available via the Internet at http://www.springer.com/chemistry/journal/11814.

REFERENCES

1. R. Sadeghbeigi, Fluid catalytic cracking handbook: An expert guide to the practical operation, design, and optimization of FCC units, Elsevier (2012).
2. W. C. Cheng, E. T. Habib, K. Rajagopalan, T. G. Roberie, R. F. Wormsbecher and M. S. Ziebarth, Fluid catalytic cracking, Handbook of Heterogeneous Catalysis (2008).
3. Z. Li, G. Wang, Y. Liu, J. Gao, C. Xu, Y. Liang and X. Wang, *Fuel Process. Technol.*, **115**, 1 (2013).
4. G. Wang, Z.-k. Li, Y.-D. Liu, J.-s. Gao, C.-m. Xu, X.-y. Lan, G.-q. Ning and Y.-m. Liang, *Ind. Eng. Chem. Res.*, **51**, 2247 (2012).
5. G. Jiménez-García, H. de Lasa, R. Quintana-Solórzano and R. Maya-Yescas, *Fuel*, **110**, 89 (2013).
6. P. O'Connor and S. Yanik, *Stud. Surf. Sci. Catal.*, **100**, 323 (1996).
7. T. Ino and S. Al-Khattaf, *Appl. Catal. A: Gen.*, **142**, 5 (1996).
8. W. Chen, D. Han, X. Sun and C. Li, *Fuel*, **106**, 498 (2013).
9. F. Leydier, C. Chizallet, A. Chaumonnot, M. Digne, E. Soyer, A.-A. Quoineaud, D. Costa and P. Raybaud, *J. Catal.*, **284**, 215 (2011).
10. I. Shimada, K. Takizawa, H. Fukunaga, N. Takahashi and T. Takatsuka, *Fuel*, **161**, 207 (2015).
11. K.-H. Lee and B.-H. Ha, *Korean J. Chem. Eng.*, **15**, 533 (1998).
12. B. Wang, C. Han, Q. Zhang, C. Li, C. Yang and H. Shan, *Energy Fuels*, **29**, 5701 (2015).
13. N. Hosseinpour, Y. Mortazavi, A. Bazyari and A. A. Khodadadi, *Fuel Process. Technol.*, **90**, 171 (2009).
14. L. Jia, X. Sun, X. Ye, C. Zou, H. Gu, Y. Huang, G. Niu and D. Zhao, *Micropor. Mesopor. Mater.*, **176**, 16 (2013).
15. X. Liu, T. Yang, P. Bai and L. Han, *Micropor. Mesopor. Mater.*, **181**, 116 (2013).
16. M. Aghakhani, A. Khodadadi, S. Najafi and Y. Mortazavi, *J. Ind. Eng. Chem.*, **20**, 3037 (2014).
17. A. Psarras, E. Iliopoulou, L. Nalbandian, A. Lappas and C. Pouwels, *Catal. Today*, **127**, 44 (2007).
18. A. Bazyari, A. Khodadadi, N. Hosseinpour and Y. Mortazavi, *Fuel Process. Technol.*, **90**, 1226 (2009).
19. G. Tonetto, J. Atias and H. De Lasa, *Appl. Catal. A: Gen.*, **270**, 9 (2004).
20. S. Al-Khattaf, J. Atias, K. Jarosch and H. De Lasa, *Chem. Eng. Sci.*, **57**, 4909 (2002).
21. S. Al-Khattaf, T. Odedairo and R. Balasamy, *Can. J. Chem. Eng.*, **91**, 607 (2013).
22. M. Falco, E. Morgado, N. Amadeo and U. Sedran, *Appl. Catal. A: Gen.*, **315**, 29 (2006).
23. K. Mahgoub and S. Al-Khattaf, *Energy Fuels*, **19**, 329 (2005).
24. R. Pujro, M. Falco and U. Sedran, *Energy Fuels*, **29**, 1543 (2015).
25. G. m. Chen, X. w. Zhang and Z. t. Mi, *J. Fuel. Chem. Technol.*, **35**, 211 (2007).
26. P. Andreu, *Catal. Lett.*, **22**, 135 (1993).
27. A. E. Beers, T. Nijhuis, N. Aalders, F. Kapteijn and J. Moulijn, *Appl. Catal. A: Gen.*, **243**, 237 (2003).

28. J. M. Zamaro, M. A. Ulla and E. E. Miró, *Chem. Eng. J.*, **106**, 25 (2005).
29. A. Beers, T. Nijhuis, F. Kapteijn and J. Moulijn, *Micropor. Mesopor. Mater.*, **48**, 279 (2001).
30. J. R. Sohn, S. J. DeCanio, P. O. Fritz and J. H. Lunsford, *J. Phys. Chem.*, **90**, 4847 (1986).
31. N. Katada, Y. Kageyama and M. Niwa, *J. Phys. Chem. B*, **104**, 7561 (2000).
32. A. F. Costa, H. S. Cerqueira, E. F. Sousa-Aguiar and M. M. Ludvig, Performance of FCC catalysts prepared with sub-micron Y zeolite, in: M. C. E. van Steen, L. H. Callanan (Eds.) Studies in Surface Science and Catalysis, Elsevier, 2296 (2004).
33. S. Sombatchaisak, P. Praserthdam, C. Chaisuk and J. Panpranot, *Ind. Eng. Chem. Res.*, **43**, 4066 (2004).
34. M. M. Kerssens, C. Sprung, G. T. Whiting and B. M. Weckhuysen, *Micropor. Mesopor. Mater.*, **189**, 136 (2014).
35. S. Al-Khattaf and H. De Lasa, *Appl. Catal. A: Gen.*, **226**, 139 (2002).
36. L. Frunz, R. Prins and G. D. Pirngruber, *Micropor. Mesopor. Mater.*, **88**, 152 (2006).
37. T.-C. Tsai, S.-B. Liu and I. Wang, *Appl. Catal. A: Gen.*, **181**, 355 (1999).
38. S. Al-Khattaf, *Energy Fuels*, **22**, 3612 (2008).
39. P. O'Connor, J. Verlaan and S. Yanik, *Catal. Today*, **43**, 305 (1998).
40. B. Wang and G. Manos, *Chem. Eng. J.*, **142**, 217 (2008).

Supporting Information

Two-stage cracking catalyst of amorphous silica-alumina on Y zeolite for enhanced product selectivity and suppressed coking

Mahdi Davoodpour*, Reza Tafreshi*, Abbas Ali Khodadadi*,,†, and Yadolla Mortazavi*,****

*Catalysis and Nanostructured Materials Research Laboratory, School of Chemical Engineering, University of Tehran, P. O. Box 11155/4563, Tehran, Iran
**Oil and Gas Center of Excellence, P. O. Box 11155/4563, University of Tehran, Tehran, Iran
(*Received 2 August 2016 • accepted 20 November 2016*)

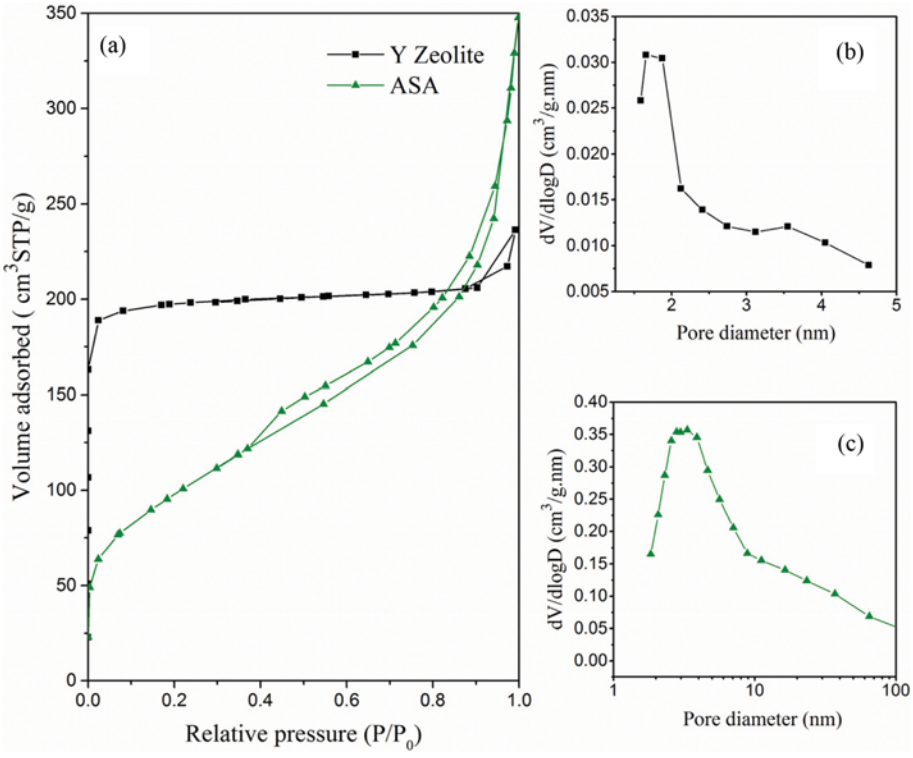

Fig. S1. N_2 adsorption-desorption isotherms of the synthesized samples (a), and the pore size distributions of (b) Y zeolite and (c) ASA.

N_2 adsorption-desorption isotherms of the synthesized Y zeolite show the common Type-I profile, indicating the microporous structure of the sample. ASA shows hysteresis in its isotherms at relatively medium to high partial pressures. This is attributed to capillary condensation in mesopores of silica-alumina. Fig. S1(b) and Fig. S1(c), respectively show the pore size distributions (PSD) for Y zeolite and ASA obtained by applying BJH method on desorption branch of N_2 isotherms. The intra-particle porosity of Y zeolite shows a peak maximum at about 1.4 nm close to the supercage diameter of its unit cell. The shoulder at about 3.5 nm is attributed to cracks and defects formed in the crystals. The PSD plot of ASA shows a broad pore size in the range of 2-100 nm. A peak maximum at about 4 nm and a shoulder at 20 nm can be marked in PSD of ASA. The peak maximum of 4 nm seems plausible for the particles with the estimated d_{BET} of 5 nm. Larger pores may be formed in particles agglomeration or binding via surface hydroxyl groups and. The mesoporosity of ASA as the matrix of RFCC catalyst, offers suitable pathways and

Table S1. Acid sites properties of the synthesized Y zeolite and amorphous silica-alumina (ASA)

Sample	Acidity (mmol NH_3/g-catalyst)			
	Total	Weak	Medium	Strong
Y zeolite	0.822	0.387 (47%)	0.401 (49%)	0.034 (4%)
ASA	0.102	0.068 (67%)	0.034 (33%)	-

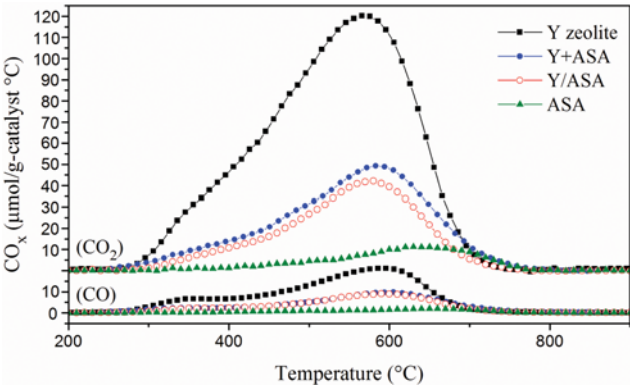

Fig. S2. CO_2 and CO evolution during TPO of coked catalysts for reaction at 350 °C and 980 s time on stream.

reaction sites for feed molecules.

The properties of acid sites of the synthesized Y zeolite and ASA are presented in terms of mmol of desorbed ammonia in Table S1. The total acidity was calculated from the area under the TPD plot. The amounts of weak, medium and strong acidities were calculated from the areas under the deconvoluted curves. The numbers in parentheses express the percentages of the total acidity.